Journal Pre-proof

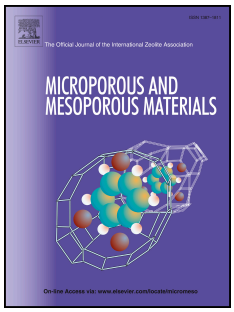

An in situ investigation of the thermal decomposition of metal-organic framework NH_2-MIL-125 (Ti)

Mian Zahid Hussain, Mounib Bahri, Werner R. Heinz, Quanli Jia, Ovidiu Ersen, Tim Kratky, Roland A. Fischer, Yanqiu Zhu, Yongde Xia

PII: S1387-1811(21)00083-4

DOI: https://doi.org/10.1016/j.micromeso.2021.110957

Reference: MICMAT 110957

To appear in: *Microporous and Mesoporous Materials*

Received Date: 8 December 2020

Revised Date: 2 February 2021

Accepted Date: 5 February 2021

Please cite this article as: M.Z. Hussain, M. Bahri, W.R. Heinz, Q. Jia, O. Ersen, T. Kratky, R.A. Fischer, Y. Zhu, Y. Xia, An in situ investigation of the thermal decomposition of metal-organic framework NH_2-MIL-125 (Ti), *Microporous and Mesoporous Materials* (2021), doi: https://doi.org/10.1016/j.micromeso.2021.110957.

CRediT authorship contribution statement:

Mian Zahid Hussain: Investigation, Methodology, Data curation; Writing - original draft. Mounib Bahri: Data curation, Validation, Writing - review & editing. Werner R. Heinz: Methodology, Data curation, Validation. Quanli Jia: Investigation, Data curation. Ovidiu Ersen: Methodology, Investigation, Data curation. Tim Kratky: Methodology, Writing - review & editing. Roland A. Fischer: Supervision, Writing - review & editing. Yanqiu Zhu: Supervision, Writing - review & editing. Yongde Xia: Supervision, Conceptualization, Methodology, Validation, Writing - review & editing.

Graphical abstract:

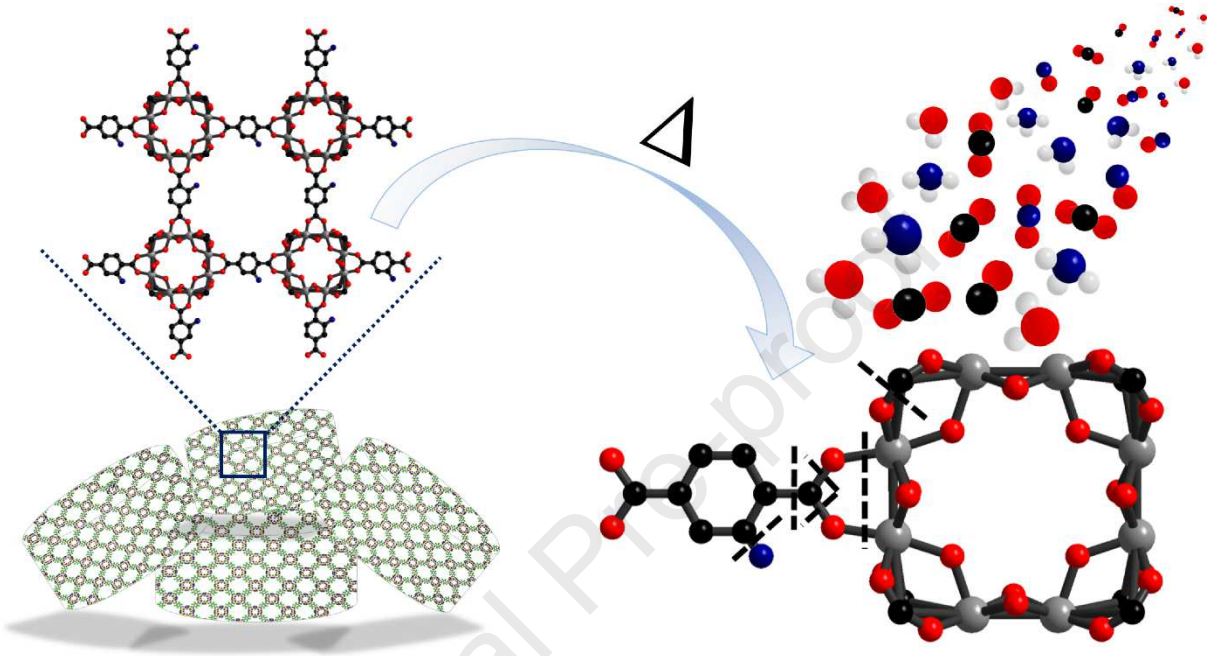

An in situ investigation of the thermal decomposition of metal-organic framework NH_2-MIL-125 (Ti)

Mian Zahid Hussain,[a, b] Mounib Bahri,[c] Werner R. Heinz,[b] Quanli Jia,[d] Ovidiu Ersen,[c] Tim Kratky,[e] Roland A. Fischer,[b] Yanqiu Zhu[a] and Yongde Xia[*a]

[a] *College of Engineering, Mathematics and Physical Sciences, University of Exeter, Exeter EX4 4QF, United Kingdom*

[b] *Department of Chemistry and Catalysis Research Centre, Technical University of Munich, Garching 85748, Germany*

[c] *Institut de Physique et Chimie des Matériaux de Strasbourg (IPCMS), UMR 7504 CNRS – Université de Strasbourg, 23 rue du Loess, 67034, Strasbourg, France*

[d] *Henan Key Laboratory of High Temperature Functional Ceramics, Zhengzhou University, Zhengzhou 450052, Henan, China*

[e] *Department of Chemistry, Technical University of Munich, Lichtenbergstraße 4, Garching 85748, Germany*

* Corresponding author.

E-mail address: Y.Xia@exeter.ac.uk (Y. Xia).

ABSTRACT

Titanium based metal-organic frameworks (MOFs) are interesting self-sacrificial precursors to derive semiconducting porous nanocomposites for highly efficient heterogeneous catalysis. However, there is a lack of systematic and in-depth mechanistic understanding of the pyrolytic conversion of MOF precursors into the desired functional composite materials. In this work, TGA-MS and in situ STEM/EDX combined with other characterization techniques were employed to investigate the evolution of the structural, physicochemical, textural and morphological properties of NH_2-MIL-125(Ti) pyrolysis at different temperatures in an inert gaseous atmosphere. In situ thermal analysis of NH_2-MIL-125(Ti) reveals the presence of 3 rather defined stages of thermal transformation in the following order: phase-pure, highly porous and crystalline MOF → intermediate amorphous phase without accessible porosity → recrystallized porous phase. The three stages occur from room temperature till 300 °C, between 350-550 °C and above ~550 °C respectively. It is found that the framework of NH_2-MIL-125(Ti) starts to collapse around 350 °C, accompanied with the cleavage of coordination and covalent bonds between organic linkers $[O_2C\text{-}C_6H_3(NH_2)\text{-}CO_2]_6$ and the Ti oxo-cluster $Ti_8O_8(OH)_4$. The organic linker continues fragmentation at 450 °C causing the shrinkage of particle sizes. The dominant pore size of 0.7 nm for NH_2-MIL-125(Ti) gradually expands to 1.4 nm at 800 °C along with the formation of mesopores. The derived disc-like particles exhibit an approximately 35% volume shrinkage compared to the pristine MOF precursor. Highly crystalline N and/or C self-doped TiO_2 nanoparticles are homogeneously distributed in the porous carbon matrix. The original 3D tetragonal disc-like morphology of the NH_2-MIL-125(Ti) remains preserved in derived N and/or C doped TiO_2/C composites. This study will provide an in-depth understanding of the thermal conversion behavior of MOFs to rationally select and design the derived composites for the relevant applications.

Keywords: MOF; TiO_2; Carbon; Nanocomposite; MOF derivative; Thermal decomposition

1. Introduction

Metal-organic frameworks (MOFs) are exceptionally porous coordination polymers fabricated by the formation of coordination bonds between organic ligands and inorganic metal clusters (called secondary building units, SBUs) with highly crystalline reticular networks.[1, 2] Since the late 1990s, MOFs have been intensively investigated for a large variety of applications such as gas separation and storage, energy storage and conversion, batteries, fuel cells, optoelectronics, sensing, supercapacitors, drug delivery and catalysis.[3-16] Recently, several studies have reported solar-light-driven applications of MOFs and derived composites.[6, 7, 12, 17-20] Despite the extraordinary surface areas and high crystallinity, relatively moderate strength of coordination bonds between constituent organic linkers and metal ions/clusters and poor semiconducting properties restrict them to be directly used for photocatalytic applications.[21-25] However, their unique properties such as rationally designed structures, a large choice of morphologies, diverse dimensions (0D, 1D, 2D and 3D, here D stands for Dimensional) together with modifiable textural properties make them excellent sacrificial templates and precursors to derive highly efficient nanocomposites.[21, 22, 26-29] Actually, all MOFs can be carbonized under appropriate pyrolysis conditions to obtain the respective metal oxides, carbides, sulfides, nitrides and phosphides embedded in a porous carbon matrix.[21, 30-32] Similar to their parental precursors, tunable MOF derived composites present great opportunity and challenge at the same time due to the multivariate parameters of design and synthesis. Therefore, it is desirable to understand the individual parameter in this complex transformation process at the atomic scale. Various studies have demonstrated that pyrolysis temperature plays the most crucial role in the rational design and optimization of desirable properties of MOF derivatives.[30, 31, 33-35] Recently, in a review Lee *et al.* summarized the experimental works on mechanistic insights of the transformation of MOFs and coordination polymers into functional nanostructures including porous metal oxides,

porous carbons and composites.[34] It was reported that the intrinsic nature of metal-ions is the key parameter that determines the phase of derived metals or compounds, and the organic linkers, as well as the synthetic conditions of the parent MOFs, are the factors that affect the possible morphology, composition, degree of graphitization and porosity of the derived carbons.[34] Although a few studies attempted to carry out in situ investigations of the decomposition processes of MOFs,[34, 36, 37] the change of crystallinity, morphology, textural and physicochemical properties of MOF during pyrolysis is still a fundamental issue to be addressed. Therefore, it is of utmost importance to further understand the transformation mechanisms of the MOF reticular structures, the evolution of porosity and simultaneous recrystallization of the metal species in the derived composites, so that to optimize the pyrolysis condition for high performing nanomaterials.

For instance, titanium-based NH_2-MIL-125(Ti) is one of the most common and stable MOFs which comprises $Ti_8O_8(OH)_4$ octamers SBUs interconnected with each six 2-amino-terephthalic acid [$(O_2C\text{-}C_6H_4(NH_2)\text{-}CO_2$] organic linkers through coordination bonds.[38] Though it is a stable 3D disc-like polymeric structure with high surface area and accessible metal sites for photocatalytic reaction, the insufficient photogeneration of electrons and poor charge transfer circumvent the material to be directly used as an efficient photocatalyst.[18, 24, 39-41] However, pyrolysis under suitable conditions can afford derived TiO_x nanoparticles or TiO_x/C nanocomposite with modifiable crystalline phases, adjustable energy band gaps, functionalized porous carbon with high surface area and tunable porosities.[18, 29, 42-44]

Herein, we present an in situ investigation of thermal conversion of NH_2-MIL-125(Ti) under an inert atmosphere. In situ STEM, TGA-MS and PXRD reveal that the reticular structure of NH_2-MIL-125(Ti) collapses at above 350 ºC due to the breaking of carboxylic and coordination bonds between Ti oxo-cluster and the NH_2-BDC organic linker. Followed by an intermediate amorphous phase between 350 and 550 ºC, recrystallization of TiO_2 takes

place at a higher temperature. At around 600 ºC the Ti oxo-cluster $Ti_8O_8(OH)_4$ in MOF precursor transform into N and/or C doped TiO_2 nanoparticles homogeneously dispersed in the porous carbon matrix. Simultaneously, the partial fragmentation of the organic linkers and the formation of carbon starts at 450 ºC that cause 35 % volume shrinkage of the MOF grain at 800 ºC, accompanied with the formation of hierarchical porosity inside the grains with relatively larger pore sizes. FTIR, Raman and XPS spectra confirmed that the chemical states of constituent elements Ti, O, C and N gradually change with an increase in pyrolysis temperatures. Interestingly, the 3D tetragonal disc-like morphology of NH_2-MIL-125(Ti) remains preserved in the derived composites. This study may provide new insights and improved understanding to rationally select the pyrolysis conditions to obtain optimized MOF derived composites with desired properties for relevant applications.

2. Experimental section

All the chemicals for the synthesis of NH_2-MIL-125(Ti) were purchased from Sigma-Aldrich and used directly without further purification.

2.1. Synthesis of NH_2-MIL-125(Ti)

NH_2-MIL-125(Ti) was synthesized by direct mixing method reported in the literature with a slight modification.[45] In a typical synthesis, 22.45 mmol of 2-aminoterephthalic acid was dissolved in a solution of 30 mL of dimethylformamide (DMF) and 30 mL of methanol (MeOH) in a 200 mL screw jar. Then, 5.5 mM (1.86 mL) of $Ti(OBu)_4$ was slowly added into the above solution and constantly stirred for 15 minutes before sealing and placing it in an oil bath at 130 ºC for 40 hours. The yellow color microcrystalline powder was collected by centrifugation followed by washing twice with DMF to remove the unreacted organic ligand

species. The same washing procedure was repeated three times with MeOH for solvent exchange. The obtained NH_2-MIL-125(Ti) was finally dried in air at 70 ºC overnight.

2.2. Thermal annealing of NH_2-MIL-125(Ti)

As-synthesized NH_2-MIL-125(Ti) was heat treated via one-step pyrolysis under an argon atmosphere at different temperatures from 200 to 900 °C. For each sample, 500 mg of NH_2-MIL-125(Ti) powder was loaded in an alumina boat and placed in the centre of a flow-through quartz tube furnace. The quartz tube was purged with argon for 30 minutes after inserting the alumina boat (with loaded sample) to ensure that the oxygen free atmosphere is established before starting the pyrolysis process. Under a constant flow (50 mL min^{-1}) of argon, the ramp rate of the tube furnace was set at 5 °C min^{-1} and the dwell time at the target temperature was 2 hours. A series of isothermally treated samples were prepared at pyrolysis temperatures of 200, 300, 400, 500, 600, 700, 800 and 900 ºC. In this work, the NH_2-MIL-125(Ti) derived TiO_2/C samples are identified and discussed with respect to their respective pyrolysis temperate.

2.3. Materials characterizations

The powder X-ray diffraction (PXRD) measurements of as-synthesized NH_2-MIL-125(Ti) and the pyrolyzed samples were performed using a Bruker D8 instrument with Cu Kα radiation (1.54 Å at 40 kV, 40 mA). Each powder sample was pressed gently on a glass slide to make a smooth surface for PXRD measurement. Thermogravimetric analysis coupled with a mass spectrometer (TGA-MS) was measured with a Mettler Toledo TGA/DSC 3 in aluminium oxide pans (70 µL with lid) with sample amounts of 1 to 5 mg. The sample was heat treated in synthetic air (20 mL min^{-1}, Westfalen, 80% N_2; 20% O_2), with ramp rate 5 °C min^{-1} from 30 °C to 1000 °C. Before starting the heating process, the sample chamber was purged with 20 mL min^{-1} synthetic air for 15 min to establish a stabilized atmosphere. For the

measurement under inert conditions, argon atmosphere was established (20 mL min^{-1}, Westfalen, 99.996%) by purging the measurement chamber with argon for 90 min at 30 °C before starting the heat treatment to ensure that the measurement chamber was completely oxygen-free. The measurement was carried out at ramp rate 5 °C min^{-1} from 30 °C to 1000 °C. After the completion of both measurements (in synthetic air and argon), another 15 min was used to stabilize the atmosphere inside the measurement chamber. Volatiles were analysed using a quadrupole mass spectrometer (MS) gas analysis system "Thermostar" from Pfeiffer Vacuum at base pressures of $\approx 10^{-7}$ mbar in multiple ion detection mode. The device was operated with *Quadera* software package. The following m/z fragments were monitored: 16 (NH_2), 17 (NH_3), 18 (H_2O), 28 (CO) 30 (NO), 44 (CO_2) and 46 (NO_2). Fourier-transform infrared (FTIR) spectra of the NH_2-MIL-125(Ti) and pyrolyzed samples (200-900 °C) were recorded using a Bruker Optics Tensor-27 FTIR spectrometer. The samples for FTIR were prepared by mixing with KBr and pressed in the form of pellets. The Raman spectra of selected samples were recorded by employing Renishaw inVia Reflex Raman System RL532C, Class 3B in a range from 20 to 2000 cm^{-1} with 1 % laser power. Scanning electron microscopy (SEM) images were taken by using the xT Nova Nanolab 600 FIB. In situ scanning transmission electron microscopy (in situ STEM) images and energy dispersive X-ray elemental mapping (EDX) of NH_2-MIL-125(Ti) were carried out by using a Jeol 2100 F FEG equipped with a spherical aberration corrector, operating at 200 kV in conventional TEM and in bright-field STEM (BF-STEM) or high-angle annular dark-field STEM (HAADF-STEM) modes with a resolution of 0.11 nm. STEM-EDX mapping was performed using a JEOL Silicon Drift Detector (DrySD60GV: sensor size 60 mm^2) with a solid angle of 0.6 srad. In situ STEM annealing under argon was carried out using a Protochips Atmosphere gas cell used as TEM holder. The sample was placed between the two SiN membranes of the micro-electrical-mechanical systems (MEMS). The temperature and the gas flow in the cell

were finely controlled by the gas delivery manifold. Before the analysis, the sample was dispersed in dichloromethane and drop-casted on the SiN membrane acting as a heater element. The in situ experiment was done at atmospheric pressure under argon. The sample was pre-heated from room temperature to 300 °C with a rate of 10 °C s^{-1} and then to 800 °C with a rate of 10 °C min^{-1}. The surface chemical analysis (X-ray photoelectron spectroscopy, XPS) of selected samples was performed on a *Leybold-Heraeus* LHS 10 spectrometer using a non-monochromatized Al-K_α source (1486.7 eV). The analyzer was operated at constant pass energy of 100 eV leading to an energy resolution with a full width at half-maximum (FWHM) of ~1.1 eV. The energy scale of the spectra was corrected by using the C1s main signal (284.6 eV, amorphous carbon). Specific surface areas and pore size distributions (PSD) of the composites were measured by N_2 sorption at 77 K on a *Quantachrome* autosorb iQ2 ASiQwin apparatus equipped with a micropore port (1×10^{-5} bar) via the conventional volumetric technique. Before the N_2 sorption analysis, the samples were evacuated/degassed at 180 ºC for 6 hours under vacuum. The PSD of the measured samples was calculated based on the adsorption branch of isotherm data by non-local density functional theory (NL-DFT) model.

3. Results and discussion

3.1. Composition and structural properties

Thermogravimetric analysis coupled with mass spectrometry (TGA-MS) was performed under oxidative (synthetic air) atmosphere as well as in inert atmosphere to study the thermal properties of NH_2-MIL-125(Ti). Though the thermal decomposition of NH_2-MIL-125(Ti) in synthetic air proceeds faster than in the inert argon atmosphere, suggesting the complete transformations of MOF precursor in air during the exothermic processes, both TGA curves

(Fig. 1a and b) show a similar four-step (**1**-**4**) decomposition pattern of NH_2-MIL-125(Ti). Under oxidative conditions in synthetic air, in stage (**1**), NH_2-MIL-125(Ti) experiences around 15 % weight loss at temperatures below 200 °C due to the removal of the residual free solvent molecules of MeOH and DMF from the pores as well as the surface absorbed moisture (H_2O), which is confirmed by the observed MS signals (Fig. 1c) with mass fragments of m/z = 18 (water), 30 (NO) and 44 (CO_2) from partially oxidized DMF. In stage (**2**) at temperatures below 280 °C, removal of the residual DMF together with the partially or fully oxidized DMF products including CO_2 and some free amino groups like carbamates or amides contribute to around 13 % of weight loss. In step (**3**) at above 350 °C up to 470 °C, a major weight loss event which can be assigned to the decomposition and oxidation of organic linkers of the framework constituents, accompanied with the formation of metal oxide particles and non-volatile macromolecular carbonaceous species, as confirmed in Fig. 1c by the emission of CO_2, NO_2, NO, NH_3 and H_2O. In step (4), the formed small amount of non-volatile macromolecular carbonaceous species are further oxidized and only TiO_2 is left as a residue. It is important to note that the temperature in Fig. 1a and b is plotted on the right hand side of Y-axis, time is plotted as the X-axis and the temperature program is in solid and dotted black line respectively. Moreover, both TGA-MS measurements in synthetic air and argon atmosphere were carried out via a similar heat up temperature program from 30 °C to 1000 °C with a ramp rate 5 °C min^{-1}. The only difference between the temperature program in synthetic air and in argon is the stabilization time at initial stage in synthetic air is only 15 minutes, but the stabilization time in argon is 90 minutes to ensure the complete removal of air/oxygen in the sample chamber.

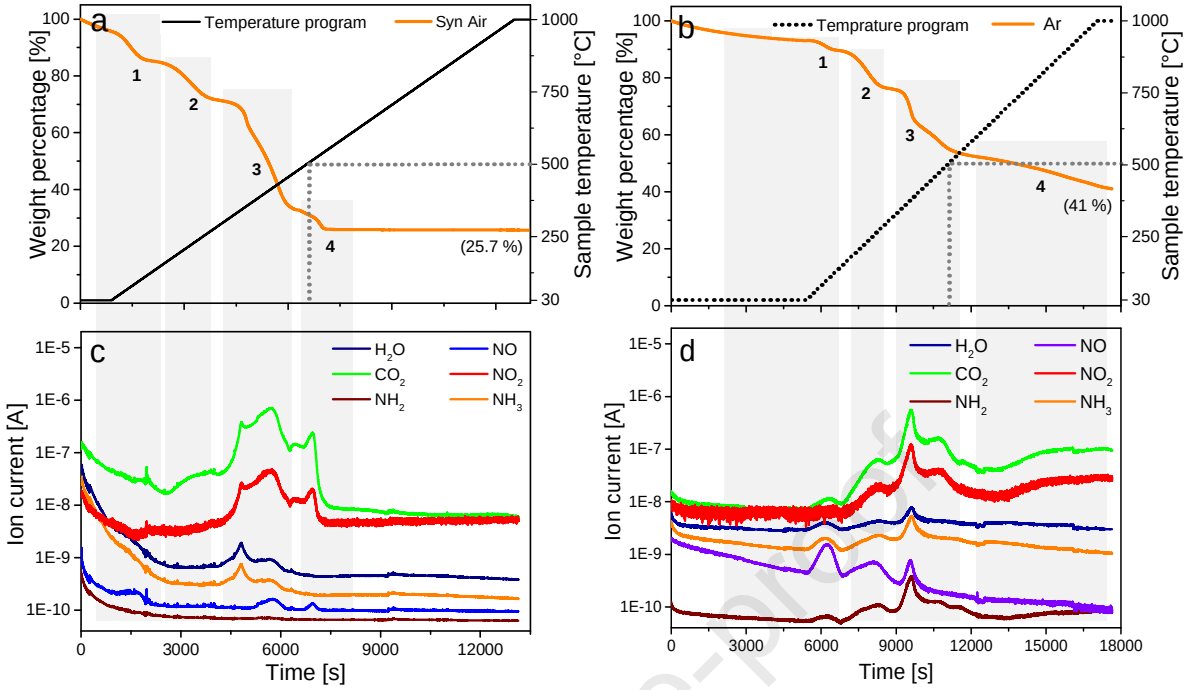

Fig. 1. TGA of NH_2-MIL-125(Ti) (a) in synthetic air and (b) in argon atmosphere. The MS of NH_2-MIL-125(Ti) (c) in synthetic air and (d) in argon atmosphere. The solid and dotted black lines in Fig 1a and b represent the temperature program in synthetic air and argon atmosphere, respectively. The horizontal and vertical grey dotted lines are only guide to suggest the temperature at a particular point.

Similar weight loss events are also observed for NH_2-MIL-125(Ti) thermolysis under argon atmosphere, but the TGA curve exhibits much less weight loss at each step and the weight loss event occurs at a relatively higher temperature, clearly suggesting the impact of the temperature and gas atmosphere on the thermal behavior of NH_2-MIL-125(Ti). In argon atmosphere, as presented in Fig. 1b, step (**3**) is different from that in synthetic air and shows only a small weight loss which may attribute to the decomposition and thermolysis of organic linkers of the framework constituents via decarbonylation, decarboxylation, dehydrogenation and even oxidation, indicating the pronounced formation of non-volatile carbonaceous phases

together with TiO_2. These intermediate non-volatile carbonaceous species slowly decompose in step (**4**) with increasing temperature up to 1000 °C, allowing cluster migration towards TiO_2 nanoparticle crystallization and transformation of amorphous carbon.

The main difference of TGA-MS of NH_2-MIL-125(Ti) in synthetic air and under argon originates from the nitrogen-containing species. Upon heat processing the precursor sample NH_2-MIL-125(Ti) in synthetic air, the -NH_2 functional group in the MOF (from NH_2-BDC) is oxidized to NO_x with m/z = 30 and 46 in step (3); while under argon atmosphere, NH_2-MIL-125(Ti) precursor does not completely change the oxidation state of the amino groups since radical NH_2 species (m/z = 16) were observed at up to 570 °C (Fig. 1d). Meanwhile, the -NH_2 group can also be eliminated as NH_3 (m/z = 17), as shown in Fig. 1d. It is worth noting that under argon atmosphere, the m/z = 30 is attributed to NO, which may be derived from the NH_2-containing organic component being partially oxidized by the presence of oxygen-containing –COOH groups in the organic linker. Based on the TGA-MS, the potential thermal decomposition mechanisms of NH_2-MIL-125(Ti) and a putative reaction equation under both atmospheres are proposed in Fig. 2.

It is worth noting that TGA is a dynamic characterization technique that uses a progressive increase of heat processing temperature of the samples, which can provide important information on the stability and the emission of volatiles species during the heating up process. However, the progressive heating process in TGA-MS analysis may result in the incompletion of the decomposition events of samples even if the process is thermodynamically favored, which may cause delayed completion of the events in TGA-MS analysis. This is in contrast to other characterization techniques such as PXRD measurements which were carried out on the isothermally treated samples. Inevitably, the exact temperatures of weight loss and decomposition events derived from TGA and XRD techniques may not be unambiguously comparable. Nevertheless, the decomposition of MOF

framework at a certain temperature windows can provide an useful indicative information of decomposition process, which are vital to support the results obtained from other characterization techniques.

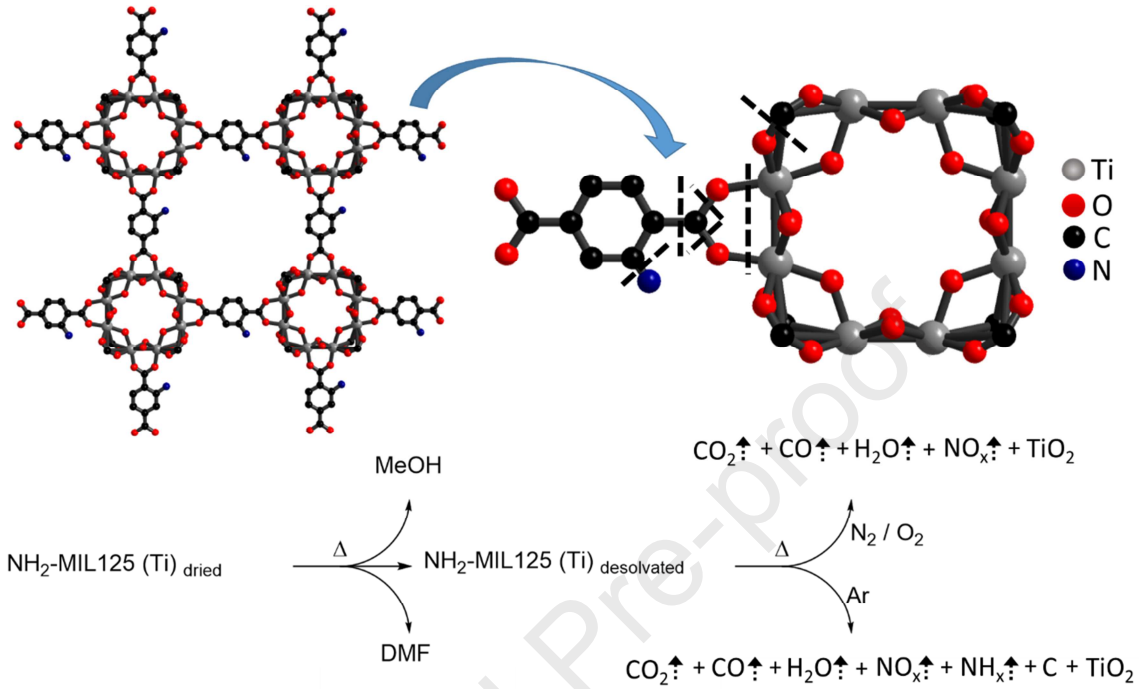

Fig. 2. A proposed scheme of thermal decomposition and putative reaction products of NH_2-MIL-125(Ti) under synthetic air and argon atmosphere based on the TGA-MS results.

The powder X-ray diffraction (XRD) patterns were recorded at ambient temperatures for all the samples. Fig. 3a clearly confirms that the precursor NH_2-MIL-125(Ti) sample at room temperature (RT) is a highly crystalline structure. The main peaks appeared at 2θ of 6.7º, 9.7º and 11.6º correspond to the simulated XRD pattern of MIL-125(Ti).[38] In this structure, six NH_2-BDC organic linker molecules interconnect the chains of μ-OH corner-shared $Ti_8O_8(OH)_4$ metal clusters, forming disc-like tetragonal 3-dimensional reticular structures shown in Fig. 2.[45, 46] Upon high-temperature pyrolysis under an argon atmosphere,

the XRD patterns of those heat treated samples from 200 to 900 °C show that the NH_2-MIL-125(Ti) network structure is stable up to 300 °C **(** inset in Fig. 3a). The decrease in peak intensity of sample heat treated at 300 °C might be related to the partial decomposition and the reorganization of the MOF structure due to the removing of hydroxo groups and the partial breaking of -NH_2 bonds, as confirmed by TGA-MS results in Fig. 1a and c. The structure of the MOF precursor is completely decomposed at above 350 °C and it forms amorphous TiO_2 from Ti oxo-cluster and porous carbon matrix from organic linkers. The XRD peaks for samples heat treated at 400 and 500 °C show no trivial peaks of NH_2-MIL-125(Ti) and the formed TiO_2 nanoparticles, suggesting the complete collapse of MOF structure and the formation of the intermediate amorphous phase of TiO_2 and carbon. Only a small hump at around 2θ of 26^o represents the formation of amorphous carbon. However, at pyrolysis temperature of 600 °C, the resulting sample shows poorly crystalline anatase TiO_2 with a broad peak emerges at 2θ of 25.2^o. The structure of NH_2-MIL-125(Ti) is stable up to 300 °C, but it disintegrates above 350 °C, followed by the recrystallization of TiO_2 nanoparticles above 550 °C. Increasing the heat processing temperature from 700 to 800 °C, well crystalline anatase and rutile peaks are observed at 2θ of 25.3^o and 27.4^o in the resulting samples respectively. However, the rutile phase in 800 °C treated sample becomes relatively more prominent compared to the anatase phase and finally, highly crystalline rutile phase dominates in the sample obtained at 900 °C with complete disappearance of the anatase phase of TiO_2. Moreover, as shown in Fig. 3b, with the increase of the heat treatment temperature from 700 to 900 °C, a small shift of the diffraction peak for rutile phase of TiO_2 towards higher 2θ can be observed in these MOF derived well crystalline TiO_2 nanoparticles sample. This shift in peak positions of rutile phase can be attributed to the modification of the crystalline structure by nitrogen and/or carbon self-doped into the TiO_2 lattice, where both

carbon and nitrogen species are derived from the NH_2-BDC organic linkers in the parental MOF precursor.[46, 47]

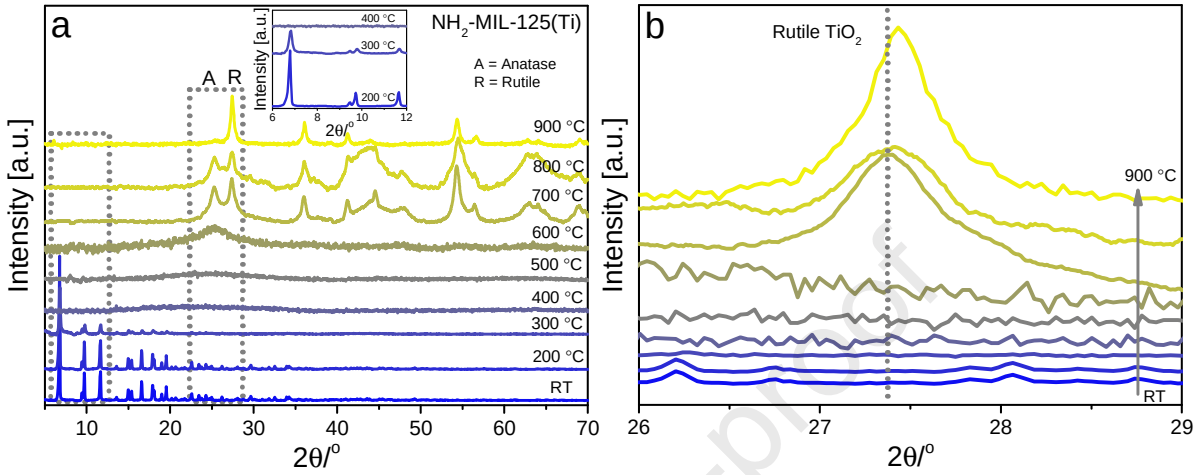

Fig. 3. (a) PXRD patterns of NH_2-MIL-125(Ti) heat treated from room temperature (RT) to 900 °C. Inset shows the XRD patterns of NH_2-MIL-125(Ti) heat treated at selected temperatures. (b) Highlighted rutile TiO_2 peaks show the shift of peak positions due to the modification of the crystalline structure.

The FTIR spectra recorded with heat pretreated samples at ambient temperatures (Fig. 4a) show the change of the chemical states of the organic linkers NH_2-BDC and the Ti-O metal clusters upon thermal processing of NH_2-MIL-125(Ti) from RT to 900 ^oC. In the as-prepared NH_2-MIL-125(Ti) precursor, a large stretching band observed at around 3400 cm^{-1} corresponds to the presence of NH_2 functional groups of the organic linker and the -OH stretching of residual solvents including methanol and water. As the heat processing temperature increases, the intensity of this band gradually decreases due to the breaking of NH_2 functional groups and the evaporation of the residual solvents. This minor stretching

band retains in samples obtained at a temperature higher than 400 °C due to the surface adsorbed moisture.[48, 49] A shoulder peak at 1710 cm^{-1} in pristine NH_2-MIL-125(Ti) can be ascribed to the stretching modes of –COOH functional groups coordinated with Ti oxo-cluster.[50, 51] The characteristic vibrational bands of carboxylate linker appear at around 1534 and 1426 cm^{-1}.[51, 52] Moreover, the peak at around 1255 cm^{-1} can be attributed to the C-N stretching modes of the aromatic amine group.[52] In pure 2-amino-terephthalic acid (NH_2-BDC), the vibrational modes are observed at around 3400, 1710 and between 1540-1250 cm^{-1} is also corresponded to NH_2, C=O (carboxylate) and C-C benzene ring respectively.[51] These vibrational bands remain unchanged up to 300 °C, confirming that no major structural change occurs in NH_2-MIL-125(Ti). However, the intensities of these peaks gradually decrease upon heating and almost disappear in samples obtained at above 400 °C due to the breaking of the carboxylate bridges and coordination bonds between NH_2-BDC linkers and the Ti (octahedra) metal cluster. Although –COOH and –NH_2 groups may break and evaporate, the aromatic rings in the organic linkers transform to carbonaceous materials and still have the benzene ring groups in the carbon materials. Above 400 °C, a strong band at around 1615 and 1385 cm^{-1} can be ascribed to the stretching vibrational modes of –C=C in the aromatic ring and bending vibrational modes of C-O-H respectively. The vibrational bands between 800-400 cm^{-1} correspond to the O-Ti-O bonds.[50] Similar to the carboxylate modes, these vibrations show no trivial variation up to 300 °C, confirming the stability of the MOF structure. With an increase of carbonization temperature to 400 °C, these sharp peaks disappear, accompanied by a broad shoulder band that can be attributed to the formation of amorphous TiO_2. However, a broader peak of crystalline TiO_2 can be observed at around 630 cm^{-1} in samples obtained at above 500 °C.[49] In accordance with the XRD results, this slight shift in the peak position (at around 630 cm^{-1}) of TiO_2 in samples obtained at temperatures from 500 to 900 °C could be ascribed to the transformation of crystalline phase from anatase to rutile and the

changes of the local chemical environment of TiO_2 nanoparticles.[46, 49] The changes in the chemical states of TiO_2 and carbon in the pyrolyzed samples were further investigated by Raman spectroscopy and X-ray photoelectron spectroscopy.

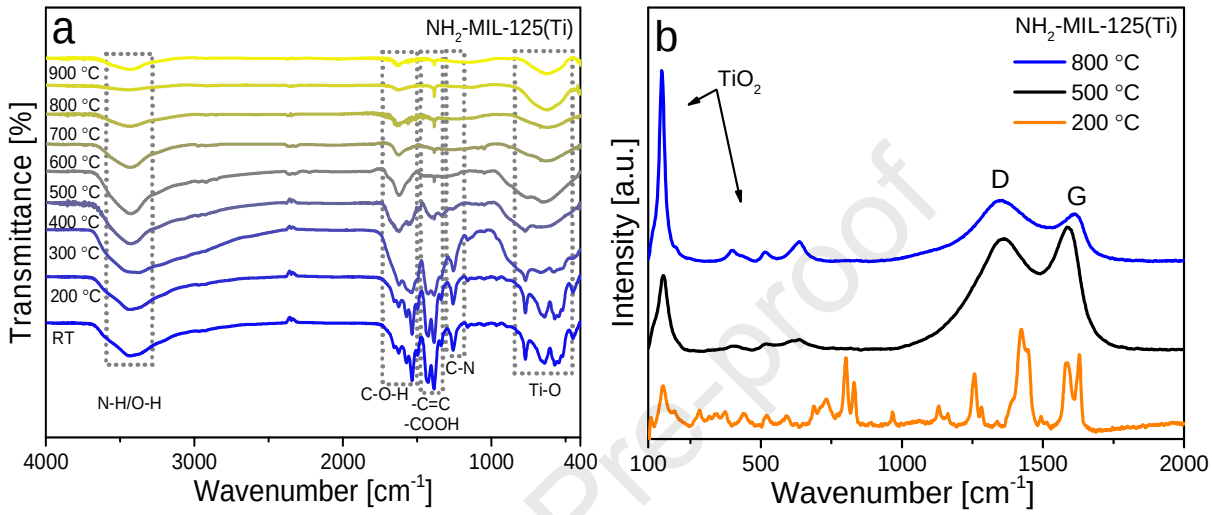

Fig. 4. (a) FTIR spectra of heat treated NH_2-MIL-125(Ti) from RT to 900 °C; (b) Raman spectra of selected samples heat treated at 200 °C (orange), 500 °C (black) and 800 °C (blue).

In Fig. 4b, the Raman spectra of selected heat treated samples are presented. The samples obtained at 500 and 800 °C show the $E_g(1)$ vibrational modes of TiO_2 at around 154 cm^{-1} and E_g vibration modes between 350-700 cm^{-1} respectively.[53, 54] The peaks appearing at 1258 and 1424 cm^{-1} in the heated treated NH_2-MIL-125(Ti) at 200 °C can be assigned to the symmetric stretching and bending modes of Ti-O-Ti-O octamer rings in the metal clusters, while the peaks appeared at around 1492 and 1630 cm^{-1} correspond to the C-C and N-H vibration modes of the organic linker (NH_2-BDC).[19, 46] However, pyrolyzing at a higher temperature, these peaks disappear and two signature peaks of D and G bands of carbon are observed in both samples obtained at 500 °C and 800 °C. The D band (breathing modes of

sp^2 hybridized carbon atoms in hexagonal rings) signifies the amorphous carbon whereas the G band (bond stretching of all sp^2 atoms in hexagonal rings and chains represents the graphitic carbon) appears due to the formation of nanocrystalline carbon.[55, 56] The D band appeared at 1368 cm^{-1} in the sample obtained at 500 °C which shifted to 1354 cm^{-1} in the sample obtained at 800 °C. Likewise, the G band was observed at 1595 cm^{-1} in sample 500 °C whereas it appeared at 1617 cm^{-1} for the sample 800 °C respectively. The blueshift in G band can be ascribed to the electronegative N functionalization, the formation of surface defects, oxygen-related defects and the diamond-like (C-C) sp^3 bonding in amorphous carbon.[56] The intensities of D and G bands suggest that carbon obtained from the pyrolysis of NH_2-MIL-125(Ti) up to 800 °C is amorphous with little graphitization.[57, 58] These observations were further confirmed by XPS results.[57-60]

The changes in chemical states of the constituent elements such as Ti, O, C and N of selected samples during the pyrolysis of the NH_2-MIL-125(Ti) were investigated by the X-ray photoelectron spectroscopy (XPS). The Ti $2p_{3/2}$ and Ti $2p_{1/2}$ peaks for sample NH_2-MIL-125(Ti) heated at 200 °C appear at 458.8 and 464.7 eV respectively (Fig. 5a). The difference in binding energies ($\Delta E_{B.E}$) of Ti $2p_{3/2}$ and Ti $2p_{1/2}$ is 5.9 eV, confirming the presence of Ti(IV) chemical state in Ti oxo-cluster.[61] However, Ti $2p_{3/2}$ and Ti $2p_{1/2}$ peaks for samples obtained at 500 and 800 °C appeared at around 458.6 and 464.6 eV respectively. The small shift in Ti $2p_{3/2}$ towards lower binding energy and the change in $\Delta E_{B.E}$ upon thermal decomposition may be attributed to the formation of TiO_2 nanoparticles,[62] although one cannot rule out this shift in the binding energy of Ti $2p_{3/2}$ might also be due to the incorporation of N and/or C atoms in TiO_2 crystal lattice substituting the O^{2-} as well as the formation of Ti^{3+} chemical states.[63-65] The O 1*s* spectra (Fig. 5b) of NH_2-MIL-125(Ti) heat treated at 200 °C can be deconvoluted into two peaks appeared at 531.9 and 531.6 eV which refer to the characteristic peaks of oxygen atoms in Ti oxo-cluster and C=O bonds

respectively.[61] However, in sample heat treated at 500 °C, the O 1s peaks appeared at 531. 3 and 530.2 eV, which can be attributed to the OH groups on the carbon surface and the signature peak of Ti-O in TiO_2 lattice respectively.[66, 67] These peaks appear at 531.2 and 530.1 eV in the sample obtained at 800 °C with a slight broadening. It confirms the growth of oxygen-related defects in TiO_2 lattice.[64, 68]

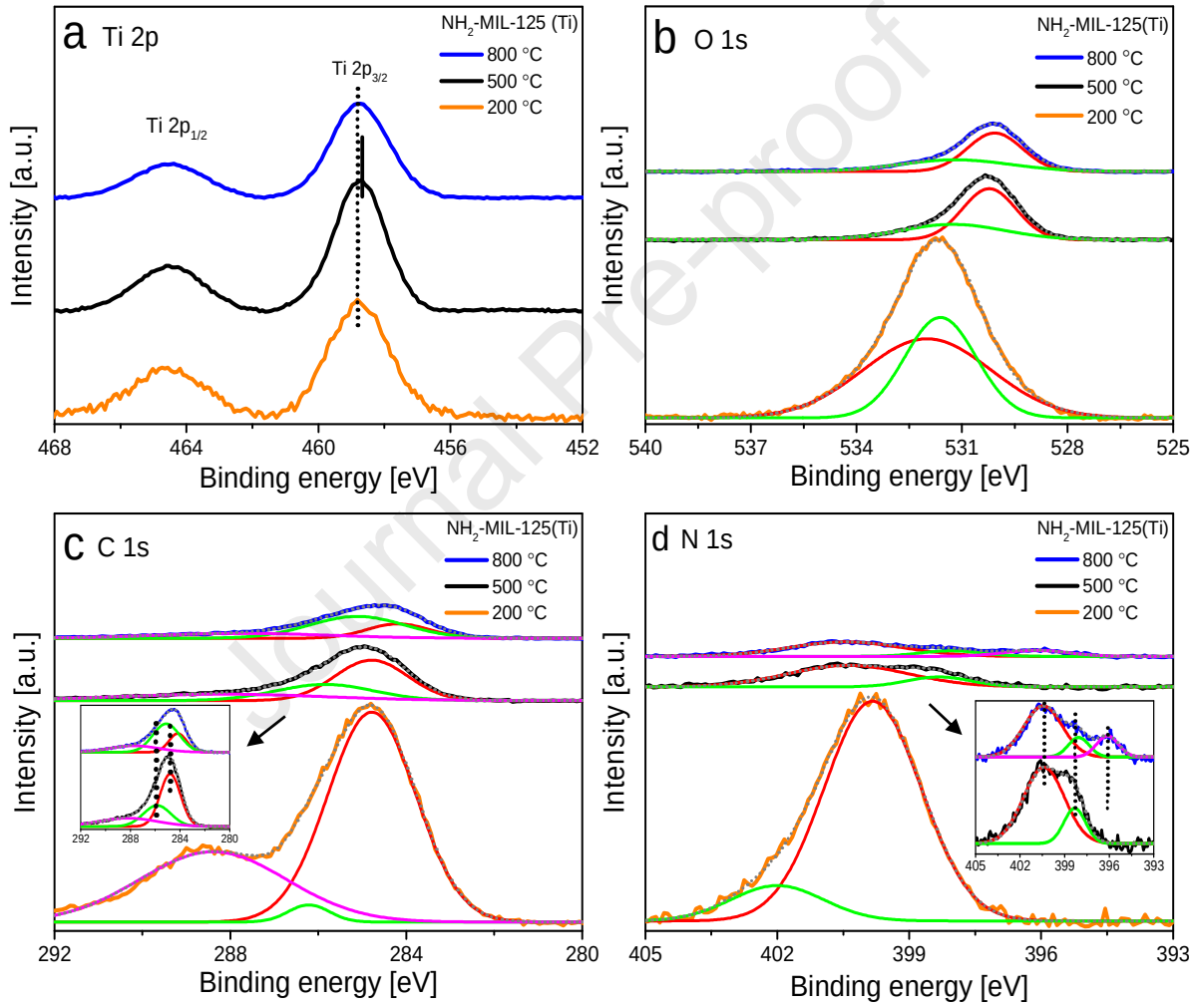

Fig. 5. XPS spectra of (a) Ti 2p, (b) O 1s, (c) C 1s and (d) N 1s of selected heat treated NH_2-MIL-125(Ti) at 200 °C (orange), 500 °C (black) and 800 °C (blue).

The deconvoluted peaks of C 1s (Fig. 5c) in NH_2-MIL-125(Ti) heated at 200 °C appear at 284.8, 286.2 and 288.4 eV which correspond to sp^2 hybridized C=C, C-O-C bonds and the O-C=O of organic linker respectively.[19, 61, 69] At 500 °C the structure of NH_2-MIL-125(Ti) completely collapsed and the organic linker transformed into the amorphous carbon. The C 1s peaks of this sample (500 °C) appeared at 284.8, 285.8 and 288.2 eV attributed to C=C, C-O and O-C=O bonds respectively.[66, 70] However, in sample obtained at 800 °C, the C 1s peaks were shifted to 284.2, 285.1 and 287.7 eV which indicate the modification in the surface chemical state of carbon species. It is worth noting that with an increase in the heat treatment temperature from 200 ^oC to 500 and 800 ^oC, the peak intensity for C 1s in the obtained samples decreased gradually, due to the less amount of C species remaining in the samples. It is also interesting to observe that the sample obtained at 800 °C showed a significant decrease in the intensity of the sp^2 hybridized C=C bond with a simultaneous increase in the intensity of the C-C bond (inset in Fig. 5c) compared to the sample obtained at 500 °C.[28, 64, 65] This is due to the growth of defects in carbon matrix and the formation of oxygen vacancies as well as a decrease in O 1s intensities with the increase of the pyrolysis temperature. This observation is in very good agreement with Raman spectra in Fig. 4b. The N1s peaks in NH_2-MIL-125(Ti) heated at 200 °C (Fig. 5d) appeared at 399.9 and 402 eV, which can be attributed to the N of the amine functional group ($-NH_2$) attached to the organic linker of NH_2-MIL-125(Ti).[71, 72] Above 380 °C, the amine functional group ($-NH_2$) cleaves off from the linker (NH_2-BDC) by breaking of C-N covalent bond under inert atmosphere as confirmed by TGA-MS, which frees the N atoms that can potentially be doped into TiO_2 lattice as well as functionalize the surface of the porous carbon. The intensity of N 1s peaks significantly decreased at high temperature indicating that most of the N evaporates in the form of NO_x under oxidative environment and in the form of NH_2/NH_3 under an inert atmosphere, as confirmed by TGA-MS results. The deconvoluted N 1s peaks in the sample

obtained at 500 °C appeared at 400.4 and 398.3 eV, which can be assigned to the pyrrolic N species and the pyridine-like N atoms presented in the porous carbon matrix respectively.[27, 73, 74] However, heating the sample to 800 °C under an argon atmosphere, along with the pyrrolic and pyridine peaks, a new peak emerged at 396.1 eV (inset in Fig. 5d) due to the substitution of N into the TiO_2 lattice. Valentin *et al.* reported that XPS N 1s core levels appear between 396-397 eV due to the substitutional N-dopants in TiO_2 representative of the Ti-N bonds.[75] This substituted N atoms replace oxygen (O^{2-}) in TiO_2 crystal lattices with N atoms signifying the formation of Ti-N bonds. These intraband states lie just above the valence band of TiO_2 that narrows down its energy band gap.[63] Based on these observations, it can be assumed that in the intermediate amorphous phase of pyrolyzed NH_2-MIL-125(Ti) sample obtained at 500 °C under an argon atmosphere, it is relatively difficult to introduce the dopants such as N atoms into TiO_2 at this temperatures. However, pyrolysis of NH_2-MIL-125(Ti) under appropriate high temperature conditions, such as heat treatment of NH_2-MIL-125(Ti) at 800 °C, can readily modify the energy band gaps and the chemical properties of the derived composites. The XPS results for all the elements are summarized in Table S1.

3.2. Textural properties

The N_2 sorption isotherms of selected samples including as-prepared NH_2-MIL-125(Ti) and samples heat treated at 200 °C, 500 °C and 800 °C were measured at 77 K to access their surface areas and pore size distributions (PSD). The PSD is calculated by the NL-DFT method based on N_2 adsorption branch data. The NH_2-MIL-125(Ti) exhibited type-I isotherm (Fig. 6a) with high adsorption below relative pressure (p/p_0) of 0.1 due to the capillary filling of micropores. The adsorption and desorption isotherms are reversible without obvious hysteresis loop, signifying the presence of predominantly uniform micropores. The activated NH_2-MIL-125(Ti) exhibits a total surface area of 1465 $m^2 g^{-1}$ with dominated microporous surface area, a pore volume of 0.6 $cm^3 g^{-1}$ and pore diameter of 0.7 nm (Fig. 6b), which is in

good agreement with literature reports.[38, 45] The sample heat treated at 200 °C showed a small hysteresis loop above relative pressure (p/p_0) of 0.4 without obvious loss of its porous characteristic. This sample possesses comparable total surface area to its precursor NH_2-MIL-125(Ti). However, it exhibited relatively decreased microporosity, accompanied with remarkably increased mesoporosity which contributes to 45% of total surface area of this sample. The emergence of mesopores and relatively higher pore volume might be due to the removal of residual solvents like DMF/MeOH and unreacted organic linkers sitting in the pore cages. Moreover, defect creation by harsh thermal activation is a known phenomenon in MOFs.[76] Interestingly, the total surface area of the sample obtained at 500 °C dropped dramatically to 157 $m^2\ g^{-1}$, due to the disintegration of the crystalline framework and the collapse of the porous structure, but one cannot rule out that the pore windows are blocked by the organic residue which prevents N_2 from accessing the pores during the gas sorption measurement. In this sample, the pore volume is reduced to 0.11 $cm^3\ g^{-1}$ and the average pore diameter is increased to 1.0 nm. However, with a further increase in heat process temperature to 800 ^oC, the obtained sample contains fully recrystallized TiO_2 nanoparticles and pyrolyzed carbonaceous species with accessible porosity. The total BET surface area of this sample obtained at 800 °C is 315 $m^2\ g^{-1}$ with a relatively decreased microporosity. This sample displays a pore volume of 0.32 $cm^3\ g^{-1}$ and pore diameter of 1.4 nm respectively. Obviously, the pore diameter of this sample (800 ºC) gradually increases with the formation of relatively larger pores at higher temperatures. As confirmed by TGA-MS and HRTEM, with the increase of pyrolysis temperature, Ti species in heat treated NH_2-MIL-125(Ti) tend to aggregate and form TiO_2 nanoparticles due to the shrinkage of the framework at higher temperature which is accompanied with the formation of porous carbon matrix. The textural properties of the precursor and heat treatment samples are summarized in Table 1. It is

evident that the BET surface area, pore volume and pore sizes of the derived composites can be finely tuned by optimizing the pyrolysis conditions.

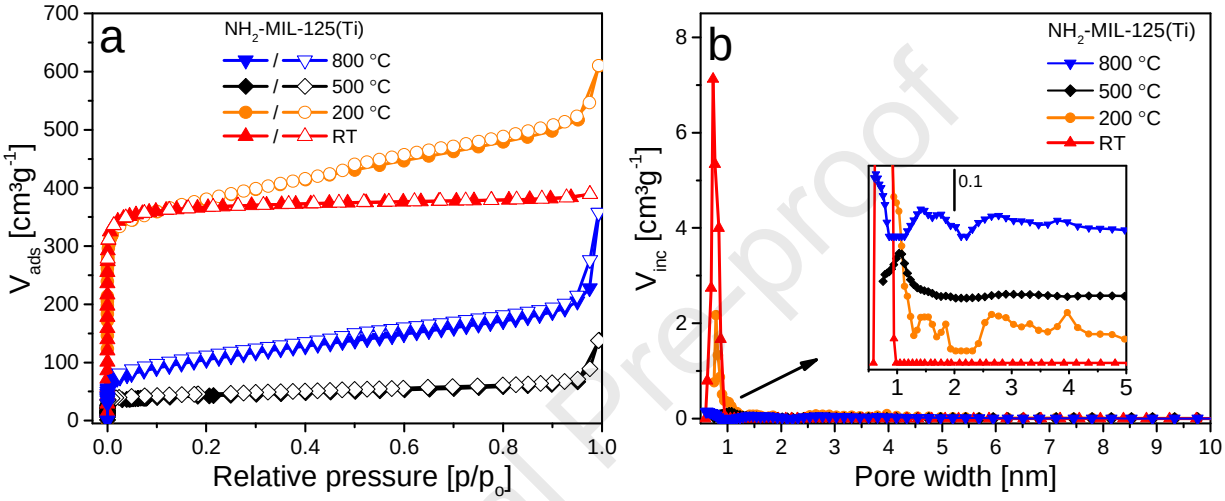

Fig. 6. (a) N_2 gas sorption isotherms and (b) PSD of as-prepared NH_2-MIL-125(Ti) (red) and samples heat treated at 200 °C (orange) 500 °C (black) and 800 °C (blue). The full and the empty symbols indicate the adsorption and desorption isotherm branch, respectively. The PSD was derived from the adsorption isotherm branch.

Table 1

Textural properties of as-prepared and heat treated NH_2-MIL-125(Ti).

NH_2-MIL-125(Ti)	Surface area ($m^2\ g^{-1}$)		Pore volume ($cm^3\ g^{-1}$)	Pore diameter (nm)
	Total surface area	Micropore surface area		
RT	1465	1336	0.60	0.7

200 °C	1435	784	0.76	0.7
500 °C	157	72	0.11	1.0
800 °C	315	47	0.32	1.4

3.3. Morphology

The in situ scanning transmission electron microscopy (STEM) images in Fig. 7 show that heating NH_2-MIL-125(Ti) in an argon atmosphere up to 300 °C has no apparent effect on the structural change and size of the crystallites. The selected particles remained almost unchanged with a particle width of 0.90 µm and apparent thickness of 0.34 µm. However, as the heat processing temperature exceeds 350 °C, the NH_2-MIL-125(Ti) reticular structure gradually loses the periodicity/crystallinity as suggested by XRD and TGA-MS results, and initiates the emission of volatile species from organic linker NH_2-BDC. It inevitably causes the shrinkage of the particle with a width of 0.74 µm and apparent thickness of 0.29 µm at around 450 °C, along with the disintegration of the metal cluster $Ti_8O_8(OH)_4$ and organic linker $[O_2C\text{-}C_6H_3(NH_2)\text{-}CO_2]_6$. Further increase of heat treatment temperature above 550 °C, the concurrently progressive evaporation of volatile species together with the formation of carbon occur for the organic linker, accompanied with more migration of metal cluster within the lattice. As a result, with the recrystallization of the metal species, the anatase phase of TiO_2 appears, which is confirmed by PXRD (Fig. 3a). As shown by TGA-MS in Fig. 1b and d, during the carbonization of NH_2-MIL-125(Ti) under argon, the residual species evaporate in the form of CO_2, NO_2, NH_3 and H_2O leaving TiO_2 nanoparticles and amorphous carbon. At 550 °C, along with the recrystallization of TiO_2, accessible porosity in carbon grains is in situ formed from the organic linker precursor, with a grain width of 0.68 µm and apparent thickness of 0.27 µm. Further increase of heat treatment temperature to 700 °C, the grain size

of the particles continues to shrink to a width of 0.64 µm with apparent thickness of 0.24 µm, along with the enlargement of the micropores as well as the gradual growth of mesopores. At 800 °C, the size of the sample exhibited approximately a volume shrinkage of 35 % and the selected particle possess a width of 0.58 µm and an apparent thickness of 0.23 µm (Fig. 7l) compared to the pristine NH_2-MIL-125(Ti). The shrinkage of the particles with the gradually increased pyrolysis temperature and the preservation of the general morphology of the precursor are clearly demonstrated via this series of the in situ STEM investigation.

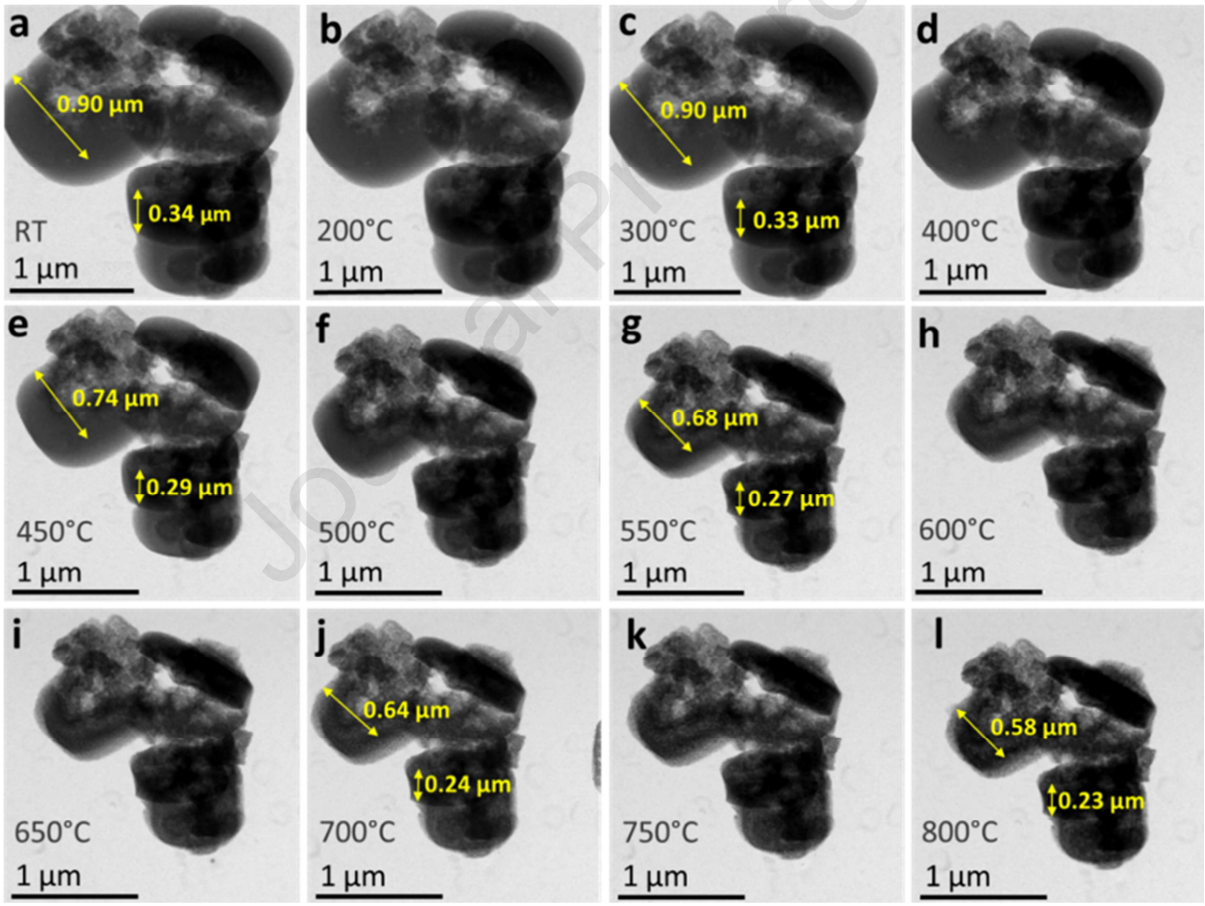

Fig. 7. In situ STEM images of samples obtained at a gradually increased heat treatment temperature of NH_2-MIL-125(Ti) under argon atmosphere.

Furthermore, as shown in Fig. S1, the SEM images of the heated treated samples indicate that the overall tetragonal 3D disc-like morphology of NH_2-MIL-125(Ti) remains preserved in the derived N and/or C doped TiO_2/C composites. Simultaneously, well crystalline anatase and rutile TiO_2 nanoparticles are uniformly immobilized in the in situ formed porous carbon matrix which is further confirmed by in situ HRTEM and EDX elemental mapping. The in situ HRTEM images of selected samples at three different pyrolysis stages such as NH_2-MIL-125(Ti) heat treated at 200 °C, the intermediate amorphous phase at 500 °C and the fully carbonized well crystalline phase at 800 °C are shown in Fig. 8. No individual Ti or TiO_2 nanoparticles are visible in sample heat treated at 200 °C (Fig. 8a and b), whereas amorphous or poorly crystalline anatase TiO_2 nanoparticles can be observed in sample heat treated at 500 °C (Fig. 8c and d). However, in the sample heated treated at 800 °C, well crystalline anatase and rutile TiO_2 nanoparticles can be seen homogeneously distributed on the surface and inside the porous carbon matrix (Fig. 8e and f). At 800 °C, the average TiO_2 particle sizes are estimated around 20 nm and lattice spacing is calculated to be 0.33 nm.[65] From these observations, it is evident that above 600 ºC, TiO_2 nanoparticles are recrystallized and form anatase phase, followed by a complete transformation into the rutile phase at 900 °C. Conventionally, metal oxides tend to form larger particles and agglomerates due to the sintering effect when heat treated at above the Tamman temperature, which is approximately half of the melting point of metal species.[21] However, the thermal decomposition of MOFs starts mostly at temperatures typically lower than the Tamman temperature of their constituent metal species (such as Ti). Therefore, once MOF decomposes, the metal cluster transforms into respective metal oxide nanoparticles. As the pyrolysis temperature increases, larger particles are formed at the expense of the smaller nanoparticles. It is interesting to observe that in NH_2-MIL-125(Ti) derived composites, the in situ formed carbon matrix constrains the mobility of the metal species and prevents them

from sintering and agglomeration, which results in a homogeneous distribution of the formed metal oxide nanoparticles embedded in high surface area porous carbon matrix.

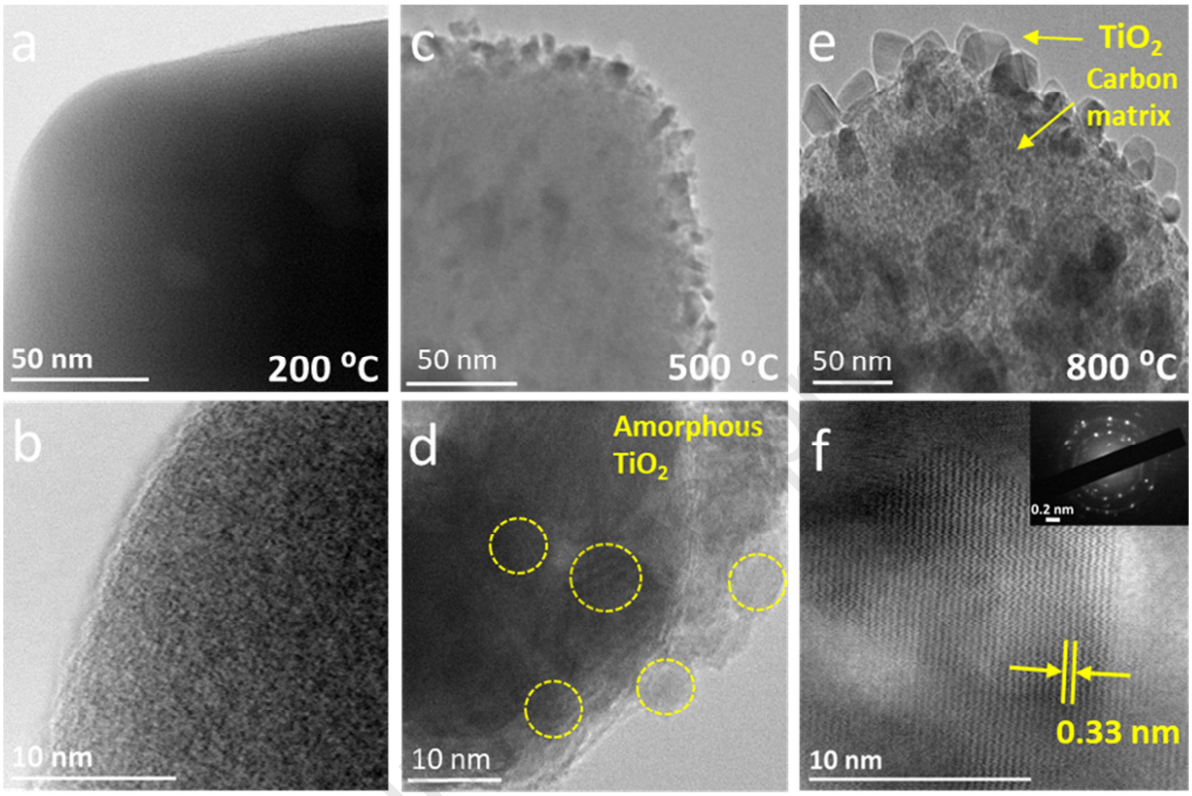

Fig. 8. HRTEM images of selected samples of NH_2-MIL-125(Ti) heat treated at (a, b) 200 °C (c, d) 500 °C and (e, f) 800 °C.

The representative in situ EDX elemental mappings of the as-prepared NH_2-MIL-125(Ti) and 800 °C heat treated samples (Fig. 9a and b) confirm that the Ti, O and C species remain homogeneously distributed throughout the whole samples.

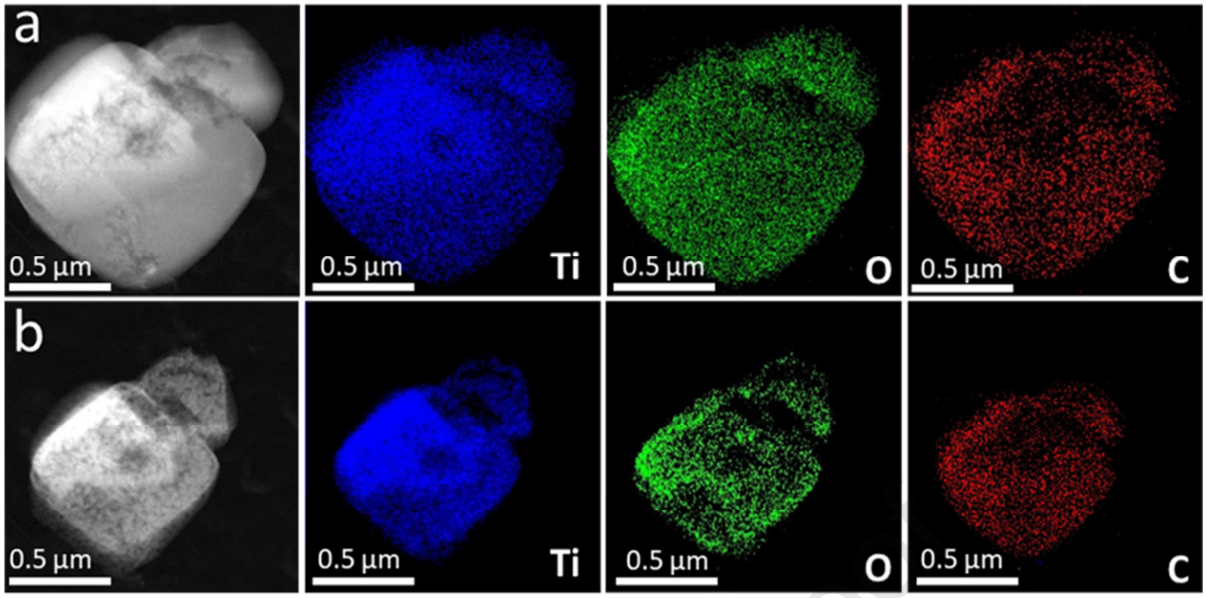

Fig. 9. In situ EDX elemental mappings of samples (a) NH_2-MIL-125(Ti) and heat treated at (b) 800 °C.

4. Conclusions

In summary, TGA-MS and in situ STEM analysis in combination with in situ EDX elemental mapping and several other characterization techniques were employed to investigate the structural, physicochemical, textural and morphological properties of as-synthesized and pyrolyzed NH_2-MIL-125(Ti). Based on the experimental observations, heat treatment of MOF, NH_2-MIL-125(Ti) under argon atmosphere results in the formation of the TiO_2/C nanocomposites via 3 stages in the following order: phase-pure, highly porous and crystalline MOF → intermediate amorphous phase without accessible porosity → recrystallized porous phase. It is revealed that the NH_2-MIL-125(Ti) framework disintegrates around 350 °C through dissociation of the organic linker $[O_2C\text{-}C_6H_3(NH_2)\text{-}CO_2]_6$ and the Ti oxo-cluster $Ti_8O_8(OH)_4$. As monitored by TGA-MS, the organic fragments gradually evaporate in the form of H_2O, CO, CO_2, NO_x and $\cdot NH_2/NH_3$. Moreover, N released via the cleavage of covalent

bonds of -NH_2 functional groups from the organic linker, not only self-doped into TiO_2 nanoparticles but also functionalizes the porous carbon. During the pyrolysis of NH_2-MIL-125(Ti), all the elements Ti, O, C and N remain homogeneously distributed in the porous carbon matrix. Pyrolysis between 350 and 550 °C, an intermediate amorphous phase is formed without accessible porosity. However, pyrolysis above 550 °C, the Ti species recrystallize and form anatase TiO_2 nanoparticles followed by the formation of well crystalline rutile TiO_2 phase above 650 °C. Simultaneously, the carbon matrix originated from the organic linker undergoes subsequent decomposition and evaporation above 450 °C causing the particle shrinkage and regenerating accessible porosity. Besides, the decomposition of organic linkers triggers fusion of the existed well-defined MOF pores into larger and less defined mesopores. The grain sizes continue to shrink and show about 35 % volume shrinkage at 800 °C compared to the pristine MOF. However, the overall morphology of the NH_2-MIL-125(Ti) remains preserved in the derived TiO_2/C composites. This study may provide new insights to rationally optimize the pyrolysis conditions for MOF derived composites to obtain the desired properties for the relevant applications.

Declaration of competing interest

The authors declare that they have no known competing financial interests or personal relationships that could have appeared to influence the work reported in this paper.

Acknowledgements

The authors are thankful to EPSRC CDT in Metamaterials at the University of Exeter for financial support. WRH thanks the Deutsche Forschungsgemeinschaft (grant no. FI-502/32-1 “DEMOFs“) and TUM Graduate School for funding.

Supplementary materials

Supplementary materials associated with this article can be found, in the online version, at https://doi.org/10.1016/j.micromeso.

References

[1] O.M. Yaghi, M. O'Keeffe, N.W. Ockwig, H.K. Chae, M. Eddaoudi, J. Kim, Nature 423 (2003) 705-714.

[2] H. Li, M. Eddaoudi, M. O'Keeffe, O.M. Yaghi, Nature 402 (1999) 276-279.

[3] J. Chen, Y. Li, Chem. Rec. 16 (2016) 1456-1476.

[4] W. Xia, A. Mahmood, R. Zou, Q. Xu, Energy Environ. Sci. 8 (2015) 1837-1866.

[5] L. Wang, Y. Han, X. Feng, J. Zhou, P. Qi, B. Wang, Coord. Chem. Rev. 307 (2016) 361-381.

[6] L. Lu, B. Wu, W. Shi, P. Cheng, Inorg. Chem. Front. 6 (2019) 3456-3467.

[7] X. Zhang, J. Wang, X.-X. Dong, Y.-K. Lv, Chemosphere 242 (2020) 125144.

[8] Q. Wang, Q. Gao, A.M. Al-Enizi, A. Nafady, S. Ma, Inorg. Chem. Front. 7 (2020) 300-339.

[9] H. Furukawa, K.E. Cordova, M. O'Keeffe, O.M. Yaghi, Science 341 (2013) 1230444.

[10] L. Feng, K.-Y. Wang, J. Powell, H.-C. Zhou, Matter 1 (2019) 801-824.

[11] X. Zhang, A. Chen, M. Zhong, Z. Zhang, X. Zhang, Z. Zhou, X.-H. Bu, Electrochem. Energy Rev. 2 (2019) 29-104.

[12] A. Kidanemariam, J. Lee, J. Park, Polymers 11 (2019).

[13] L. Li, J. He, Y. Wang, X. Lv, X. Gu, P. Dai, D. Liu, X. Zhao, J. Mater. Chem. A 7 (2019) 1964-1988.

[14] C.-C. Wang, J.-R. Li, X.-L. Lv, Y.-Q. Zhang, G. Guo, Energy Environ. Sci. 7 (2014) 2831-2867.

[15] R. Medishetty, J.K. Zaręba, D. Mayer, M. Samoć, R.A. Fischer, Chem. Soc. Rev. 46 (2017) 4976-5004.

[16] H. Wang, S.I. Vagin, S. Lane, W. Lin, V. Shyta, W.R. Heinz, C. Van Dyck, A.J. Bergren, K. Gardner, B. Rieger, A. Meldrum, Chem. Mater. 31 (2019) 5816-5823.

[17] F. Song, W. Li, Y. Sun, Inorganics 5 (2017).

[18] Z. Xie, W. Xu, X. Cui, Y. Wang, ChemSusChem 10 (2017) 1645-1663.

[19] P. Karthik, R. Vinoth, P. Zhang, W. Choi, E. Balaraman, B. Neppolian, ACS Appl. Energy Mater. 1 (2018) 1913-1923.

[20] B. Zhang, J. Zhang, X. Tan, D. Shao, J. Shi, L. Zheng, J. Zhang, G. Yang, B. Han, ACS Appl. Mater. Interfaces 10 (2018) 16418-16423.

[21] L. Oar-Arteta, T. Wezendonk, X. Sun, F. Kapteijn, J. Gascon, Mater. Chem. Front. 1 (2017) 1709-1745.

[22] S. Dang, Q.-L. Zhu, Q. Xu, Nat. Rev. Mater. 3 (2017) 17075.

[23] C.H. Hendon, A.J. Rieth, M.D. Korzynski, M. Dinca, ACS Cent. Sci. 3 (2017) 554-563.

[24] M.A. Nasalevich, M. van der Veen, F. Kapteijn, J. Gascon, CrystEngComm 16 (2014) 4919-4926.

[25] D. Li, H.-Q. Xu, L. Jiao, H.-L. Jiang, EnergyChem 1 (2019) 100005.

[26] Y. Song, X. Li, L. Sun, L. Wang, RSC Adv. 5 (2015) 7267-7279.

[27] Z. Huang, Z. Yang, M.Z. Hussain, B. Chen, Q. Jia, Y. Zhu, Y. Xia, Electrochim. Acta 330 (2020) 135335.

[28] M.Z. Hussain, G.S. Pawar, Z. Huang, A.A. Tahir, R.A. Fischer, Y. Zhu, Y. Xia, Carbon 146 (2019) 348-363.

[29] X. Cao, C. Tan, M. Sindoro, H. Zhang, Chem. Soc. Rev. 46 (2017) 2660-2677.

[30] W. Zhan, L. Sun, X. Han, NanoMicro Lett. 11 (2019) 1.

[31] T. Chen, X. Liu, L. Niu, Y. Gong, C. Li, S. Xu, L. Pan, Inorg. Chem. Front. 7 (2020) 567-582.

[32] Y. Liu, X. Xu, Z. Shao, S.P. Jiang, Energy Storage Mater. 26 (2020) 1-22.

[33] W. Sun, X. Tang, Y. Wang, Electrochem. Energy Rev. 3 (2020) 127-154.

[34] K.J. Lee, J.H. Lee, S. Jeoung, H.R. Moon, Acc. Chem. Res. 50 (2017) 2684-2692.

[35] W.R. Heinz, I. Agirrezabal-Telleria, R. Junk, J. Berger, J. Wang, D.I. Sharapa, M. Gil-Calvo, I. Luz, M. Soukri, F. Studt, Y. Wang, C. Wöll, H. Bunzen, M. Drees, R.A. Fischer, ACS Appl. Mater. Interfaces 12 (2020) 40635-40647.

[36] L. Zhang, Y.H. Hu, J. Phys. Chem. C 114 (2010) 2566-2572.

[37] K. He, Z. Cao, R. Liu, Y. Miao, H. Ma, Y. Ding, Nano Res. 9 (2016) 1856-1865.

[38] M. Dan-Hardi, C. Serre, T. Frot, L. Rozes, G. Maurin, C. Sanchez, G. Férey, J. Am. Chem. Soc. 131 (2009) 10857-10859.

[39] H. Wang, Q.-L. Zhu, R. Zou, Q. Xu, Chem 2 (2017) 52-80.

[40] M.A. Nasalevich, R. Becker, E.V. Ramos-Fernandez, S. Castellanos, S.L. Veber, M.V. Fedin, F. Kapteijn, J.N.H. Reek, J.I. van der Vlugt, J. Gascon, Energy Environ. Sci. 8 (2015) 364-375.

[41] L. Zeng, X. Guo, C. He, C. Duan, ACS Catal. 6 (2016) 7935-7947.

[42] S.J. Yang, J.H. Im, T. Kim, K. Lee, C.R. Park, J. Hazard. Mater. 186 (2011) 376-382.

[43] Y.-Z. Chen, R. Zhang, L. Jiao, H.-L. Jiang, Coord. Chem. Rev. 362 (2018) 1-23.

[44] F. Marpaung, M. Kim, J.H. Khan, K. Konstantinov, Y. Yamauchi, M.S.A. Hossain, J. Na, J. Kim, Chem. Asian J. 14 (2019) 1331-1343.

[45] M. Sohail, Y.-N. Yun, E. Lee, S.K. Kim, K. Cho, J.-N. Kim, T.W. Kim, J.-H. Moon, H. Kim, Cryst. Growth Des. 17 (2017) 1208-1213.

[46] S. Hu, M. Liu, K. Li, Y. Zuo, A. Zhang, C. Song, G. Zhang, X. Guo, CrystEngComm 16 (2014) 9645-9650.

[47] Z. Luo, A.S. Poyraz, C.-H. Kuo, R. Miao, Y. Meng, S.-Y. Chen, T. Jiang, C. Wenos, S.L. Suib, Chem. Mater. 27 (2014) 6-17.

[48] M.Z. Hussain, B. van der Linden, Z. Yang, Q. Jia, H. Chang, R.A. Fischer, F. Kapteijn, Y. Zhu, Y. Xia, J. Mater. Chem. A 9 (2021) DOI: 10.1039/d0ta10853g.

[49] M.Z. Hussain, Z. Yang, B. van der Linden, Z. Huang, Q. Jia, E. Cerrato, R.A. Fischer, F. Kapteijn, Y. Zhu, Y. Xia, J. Energy Chem. 57 (2021) 485-495.

[50] A. Gómez-Avilés, M. Peñas-Garzón, J. Bedia, D.D. Dionysiou, J.J. Rodríguez, C. Belver, Appl. Catal. B 253 (2019) 253-262.

[51] M. Karabacak, M. Cinar, Z. Unal, M. Kurt, J. Mol. Struct. 982 (2010) 22-27.

[52] M. Oveisi, M.A. Asli, N.M. Mahmoodi, J. Hazard. Mater. 347 (2018) 123-140.

[53] O. Frank, M. Zukalova, B. Laskova, J. Kürti, J. Koltai, L. Kavan, Phys. Chem. Chem. Phys. 14 (2012) 14567-14572.

[54] W.F. Zhang, Y.L. He, M.S. Zhang, Z. Yin, Q. Chen, J. Phys. D: Appl. Phys. 33 (2000) 912.

[55] P.K. Chu, L. Li, Mater. Chem. Phys. 96 (2006) 253-277.

[56] A.C. Ferrari, J. Robertson, Phys. Rev. B 61 (2000) 14095-14107.

[57] Y. Gong, Y. Tang, Z. Mao, X. Wu, Q. Liu, S. Hu, S. Xiong, X. Wang, J. Mater. Chem. A 6 (2018) 13696-13704.

[58] H. Karimi, M.A. Heidari, H.B.M. Emrooz, M. Shokouhimehr, Diam. Relat. Mater. 108 (2020) 107999.

[59] J. Schwan, S. Ulrich, V. Batori, H. Ehrhardt, S.R.P. Silva, J. Appl. Phys. 80 (1996) 440-447.

[60] R.E. Shroder, R.J. Nemanich, J.T. Glass, Phys. Rev. B 41 (1990) 3738-3745.

[61] Q. Wang, G. Wang, X. Liang, X. Dong, X. Zhang, Appl. Surf. Sci. 467-468 (2019) 320-327.

[62] N.C. Saha, H.G. Tompkins, J. Appl. Phys. 72 (1992) 3072-3079.

[63] R. Asahi, T. Morikawa, T. Ohwaki, K. Aoki, Y. Taga, Science 293 (2001) 269-271.

[64] D.H. Wang, L. Jia, X.L. Wu, L.Q. Lu, A.W. Xu, Nanoscale 4 (2012) 576-584.

[65] Z. Guo, J.K. Cheng, Z. Hu, M. Zhang, Q. Xu, Z. Kang, D. Zhao, RSC Adv. 4 (2014) 34221-34225.

[66] P. Iamprasertkun, A. Krittayavathananon, M. Sawangphruk, Carbon 102 (2016) 455-461.

[67] X. Song, W. Li, D. He, H. Wu, Z. Ke, C. Jiang, G. Wang, X. Xiao, Adv. Energy Mater. 8 (2018) 1800165.

[68] T.C. Jagadale, S.P. Takale, R.S. Sonawane, H.M. Joshi, S.I. Patil, B.B. Kale, S.B. Ogale, J. Phys. Chem. C 112 (2008) 14595-14602.

[69] F. Li, D. Wang, Q.-J. Xing, G. Zhou, S.-S. Liu, Y. Li, L.-L. Zheng, P. Ye, J.-P. Zou, Appl. Catal. B 243 (2019) 621-628.

[70] M.Z. Hussain, A. Schneemann, R.A. Fischer, Y. Zhu, Y. Xia, ACS Appl. Energy Mater. 1 (2018) 4695-4707.

[71] D. Ao, J. Zhang, H. Liu, J. Photochem. Photobiol. A Chem. 364 (2018) 524-533.

[72] J. Qiu, L. Yang, M. Li, J. Yao, Mater. Res. Bull. 112 (2019) 297-306.

[73] F. Kapteijn, J.A. Moulijn, S. Matzner, H.P. Boehm, Carbon 37 (1999) 1143-1150.

[74] J.R. Pels, F. Kapteijn, J.A. Moulijn, Q. Zhu, K.M. Thomas, Carbon 33 (1995) 1641-1653.

[75] C. Di Valentin, E. Finazzi, G. Pacchioni, A. Selloni, S. Livraghi, M.C. Paganini, E. Giamello, Chem. Phys. 339 (2007) 44-56.

[76] S. Dissegna, K. Epp, W.R. Heinz, G. Kieslich, R.A. Fischer, Adv. Mater. 30 (2018) 1704501.

Highlights:

- A number of techniques used in the characterization of the MOF decomposition process.
- Some characterization techniques were carried out in situ to study MOF decomposition.
- MOF NH_2-MIL-125 (Ti) thermally decomposes to composites via 3 well defined stages.
- TiO_2/C with developed mesopores maintains particle shapes with 35% sizes shrinkage.

Declaration of interests

☒ The authors declare that they have no known competing financial interests or personal relationships that could have appeared to influence the work reported in this paper.

☐The authors declare the following financial interests/personal relationships which may be considered as potential competing interests: